Global modeling of the lower three polyads of PH_3
Preliminary results

A.V. Nikitin[a], J.-P. Champion[b], R.A.H. Butler[c], L.R. Brown[d], I. Kleiner[e]

December 22, 2008

[a]Laboratory of Theoretical Spectroscopy, Institute of Atmospheric Optics, Russian Academy of Sciences, 634055 TOMSK, Russia. [b]Institut Carnot de Bourgogne, UMR 5209 CNRS - Université de Bourgogne, 9 Av. A. Savary, BP 47870, F-21078 DIJON Cedex, France. [c]Pittsburg State University, PITTSBURG, KS 66762 USA. [d]Jet Propulsion Laboratory, California Institute of Technology, 4800 Oak Grove Drive, CA 91109, PASADENA, USA. [e]Laboratoire Inter-Universitaire des Systèmes Atmosphériques, CNRS - Universités Paris 7 et Paris 12, 61 Av. général de Gaulle, 94010 CRETEIL Cedex, France

Abstract

In order to model the high-resolution infrared spectrum of the phosphine molecule in the 3 μm region, a global approach involving the lower three polyads of the molecule (Dyad, Pentad and Octad) as been applied using an effective hamiltonian in the form of irreducible tensors. This model allowed to describe all the 15 vibrational states involved and to consider explicitly all relevant ro-vibrational interactions that cannot be accounted for by conventional perturbation approaches.2245 levels (up to $J = 14$) observed through transitions arising from 34 cold and hot bands including all available existing data as well as new experimental data have been fitted simultaneously using a unique set of effective hamiltonian parameters. The rms achieved is 0.63×10^{-3} cm^{-1} for 450 Dyad levels, 1.5×10^{-3} cm^{-1} for 1058 Pentad levels (from 3585 transitions) and 4.3×10^{-3} cm^{-1} for 737 Octad levels (from 2243 transitions). This work represents the first theoretical modeling of the 3 μm region. It also improves the modeling of the region around 4.5 μm by dividing the rms reported by previous works by a factor 6. A preliminary intensity analysis based on consistent sets of effective dipole moment operators for cold and hot bands has been simultaneously undertaken for direct comparison between observed and modeled absorption from 700 to 3500 cm^{-1}.

Keywords : Phosphine ; PH_3 ; Vibrational polyads ; Global modeling ; Near infrared ; High-resolution ; Positions ; Intensities

1 Introduction

As part of extensive efforts to support remote sensing of Jupiter and Saturn many works have been devoted to the high-resolution infrared spectrum of phosphine [1, 2, 3, 4, 5, 6, 7]. Recent works focused on the 3 μm region reported experimental measurements and assignments [5, 7], but so far no comprehensive modeling was reported.

Table 1: Experimental data for global modeling of the PH_3 polyads

Region (cm^{-1})	Dyad (800 – 1350)	Pentad (1750 – 2600)	Octad (2700 – 3600)
Spectrometers (Resolution / cm^{-1})	Bomem FTS (0.004) PNNL FTS (0.003) [32]	Orsay FTS (0.0054)	Kitt Peak FTS (0.011)
# of positions available	2490 Fusina / Di Lonardo [2]	3766 Tarrago et al. [1]	$\sim$ 8000 Butler et al. [7]
Precision (cm^{-1})	0.0001	$\sim$ 0.0010–	0.0005 to 0.0050
Calibration standard	N_2O, OCS Maki and Wells [22]		CO (2-0) Pollock et al. [23]
Intensities from these works	$\sim$ 1100 Brown et al. [4]	$\sim$ 1600 obs. Used Calc. [1]	$\sim$ 8000 Butler et al. [7]
Precision %	1.5 to 5	10 -	2 to 20
Additional values for present study	New line positions retrieved from PNNL (for Pentad–Dyad) and Kitt Peak spectra (for Pentad). Assignment aided using Kitt Peak spectra at 200–220 K ; 1–3 torr pressures ; 4.25 to 16.3 m path		

FTS : Fourier transform spectrometer; PNNL : Pacific Northwest National Laboratory in Washington, USA; Orsay : Guelachvili in France; Kitt Peak : McMath Pierce at Kitt Peak National Observatory in Arizona, USA.

At present, the line parameters of phosphine (positions and intensities) in the 3 μm region rely essentially on the empirical database reported in Ref. [7] and included in HITRAN [8] and GEISA [9]. In the spectral region from 2700 to 3500 cm^{-1}, the HITRAN compilation contains over 3000 unassigned PH_3 lines with intensities ranging from $1. \times 10^{-25}$ to 1.5×10^{-22} cm$\times$molecule^{-1}. Moreover, only one hot band arising from the upper state of ν_2 is included. The main reason for this lack of modeling is the fundamental limitation of conventional perturbation approaches. So far, only weakly interacting features could be fitted using isolated band models while strongly interacting states were left out. In fact, apart from degeneracy considerations, due to the quasi spherical character of the inertia tensor of the molecule and to specific quasi coincidences among its vibrational fundamental frequencies, the vibrational pattern of the phosphine molecule is quite similar to that of the methane molecule. The phosphine molecule was then a good candidate for the global approach successfully developed for spherical tops [10, 11] and extensively applied to other complex band systems encountered in polyatomic molecules [12, 13, 14]. The vibrational spectrum of PH_3 and its isotopomers has also been investigated by *ab initio* calculations [15, 16, 17, 18]. Recent works have reported *ab initio* vibrational energies [19, 20] and theoretical transition moments [21]. The experimental data involved in the present work are described in the next section. Then section 3 is devoted to the description of the global effective model by focusing on both similarities and peculiarities with respect to previous studies. The results are finally presented and discussed in section 4. A major emphasis of the present study is to advance the assignment of the Octad using cold and hot band transitions and modeling of the corresponding line positions. Some preliminary examination of the line intensities was performed in order to interpret the spectrum.

2 Experimental details

The present global study essentially used experimental data already exploited in previous separate works [1, 2, 3, 4, 7]. Table 1 provides an overview of measurements used for each PH_3 polyad. Previously assigned data for

Figure 1: Experimental overview spectrum of phosphine at 3 μm and 5 μm

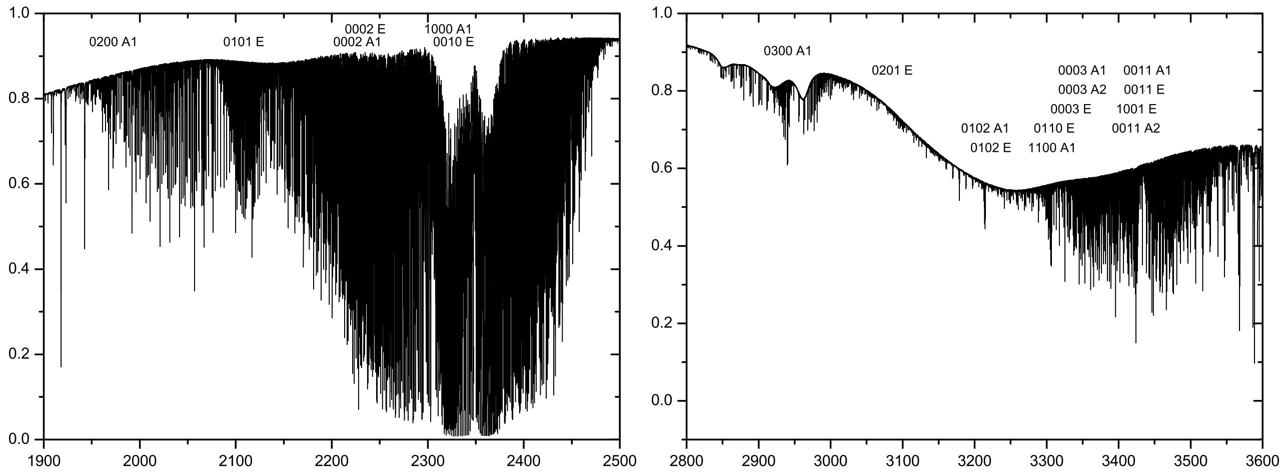

Spectrum recorded using the Kitt Peak FTS at 0.0115 cm^{-1} with a path length of 4.25 m and a pressure of 2.46 torr at 210 K .

the Dyad and Pentad systems were directly transferred into our present model, as described in section 4. For simplicity, the ground state constants and merged observed upper state levels of the Dyad from Fusina and Di Lonardo [2] were utilized. Computer files of the more recent Dyad [4] and Octad [7] data were readily available, but for the Tarrago et al. [1] 1992 Pentad study, only the line positions used in the modeling could be accessed electronically.

The Kitt Peak spectra had been recorded specifically for the Octad study, but as seen in Fig. 1, these data also provided some information on the overtone and combination bands of the Pentad. The fundamentals were too absorbing to be well measured in these data, however. The corresponding experimental conditions of these spectra were given in Table 1 of [7]. In such dense spectral regions, predictions of line positions alone are often insufficient to extend assignments. We therefore attempted some preliminary modeling of available line intensities and also inspected a few low temperature scans near 210 K in order to extend the analysis to higher J. Because the measured Pentad intensities from Tarrago et al. were not available, we treated the calculated Pentad intensities on HITRAN [8] as observed data. The simultaneous fit of data from different spectral regions and different instrumental origins (cold and hot bands) requires also special attention to calibration consistency. The positions from Dyad [2] and Octad [7] had been calibrated using reliable frequency standards (Dyad: OCS and N_2O from Maki and Wells [22]; Octad: 2−0 CO from Pollock et al. [23]), but the calibration standard used by Tarrago et al. [1] for the Pentad positions was not given. Nevertheless, the observed $2\nu_2$ positions from Tarrago were consistent within 0.001 cm^{-1} with values retrieved from Kitt Peak PH_3 spectra calibrated using the 1−0 band of CO [22].

3 Theoretical model

As mentioned in the introduction, due to the quasi spherical character of the phosphine molecule, the model used in the present work is formally the same as the model used for the similar global analysis of the methane molecule reported recently [24]. A detailed description of the main theoretical features can be found in the original paper [10] and in subsequent reviews [14, 25]. This approach has been already successfully applied to complex band systems of symmetric top molecules like CH_3D [26, 27, 28] and CH_3Cl [29, 30]. Only basic or original features with respect to previous works will be repeated or detailed here.

The polyad structure of the phosphine molecule is essentially governed by the quasi coincidence of the stretching fundamental frequencies with the first overtones of the bending frequencies following the simple approximate relation below which differs from the one for methane only by the symmetries (or equivalently by the degeneracies)

$$\nu_1(A_1) \simeq \nu_3(E) \simeq 2\nu_2(A_1) \simeq 2\nu_4(E). \tag{1}$$

The polyads P_n are defined by an integer n expressed in terms of the principal vibrational quantum numbers as

$$n = 2(v_1 + v_3) + v_2 + \nu_4. \tag{2}$$

Reduced ro-vibrational energy diagrams of the phosphine molecule are plotted in Fig. 2 and the corresponding intensities are shown in Fig. 3. In these diagrams the colors (web version) are assigned according to the principal eigenvector coefficients providing an overall picture of the effects of intra-polyad ro-vibrational interactions. The band origins ($J = 0$) of the 21 vibrational substates involved in the present study are quoted in Table 2. Recent independent *ab initio* values [19, 20] are reported for comparison. The partially transformed ro-vibrational hamiltonian adapted to the polyad structure of the PH_3 molecule (formally identical to the one of the CH_4 molecule [24]) is expressed as

$$\mathcal{H} = \mathcal{H}_{\{G.S.\}} + \mathcal{H}_{\{Dyad\}} + \mathcal{H}_{\{Pentad\}} + \mathcal{H}_{\{Octad\}} + \dots \tag{3}$$

where the subsequent terms correspond to the successive polyads with increasing vibrational energies. Each group contains a series of terms identified by rotational, vibrational and symmetry indices according to the generic nomenclature

$$t^{\Omega_r(K,\kappa C)}_{n_1n_2n_3n_4,m_1m_2m_3m_4} T^{\Omega_r(K,\kappa C)}_{n_1n_2n_3n_4,m_1m_2m_3m_4}, \tag{4}$$

where $T^{\cdots}_{\cdots}$ designates a tensor operator and $t^{\cdots}_{\cdots}$ the corresponding adjustable parameter.

The upper indices indicate the rotational characteristics of the considered term : Ω_r is the rotational power with respect to the angular momentum components J_α ; K is the tensor rank in the full rotation group ; C is the rotational symmetry coinciding with the vibrational symmetry to satisfy the invariance condition under the molecular point group operations ; κ indicates the maximum ΔK of the matrix elements. The lower indices n_i and m_i ($i = 1, ..., 4$) are respectively the powers of creation and annihilation vibrational operators associated with the four normal modes of the molecule. The total vibrational power Ω_v is given by

Figure 2: Reduced energy diagrams of the PH_3 Dyad, Pentad and Octad

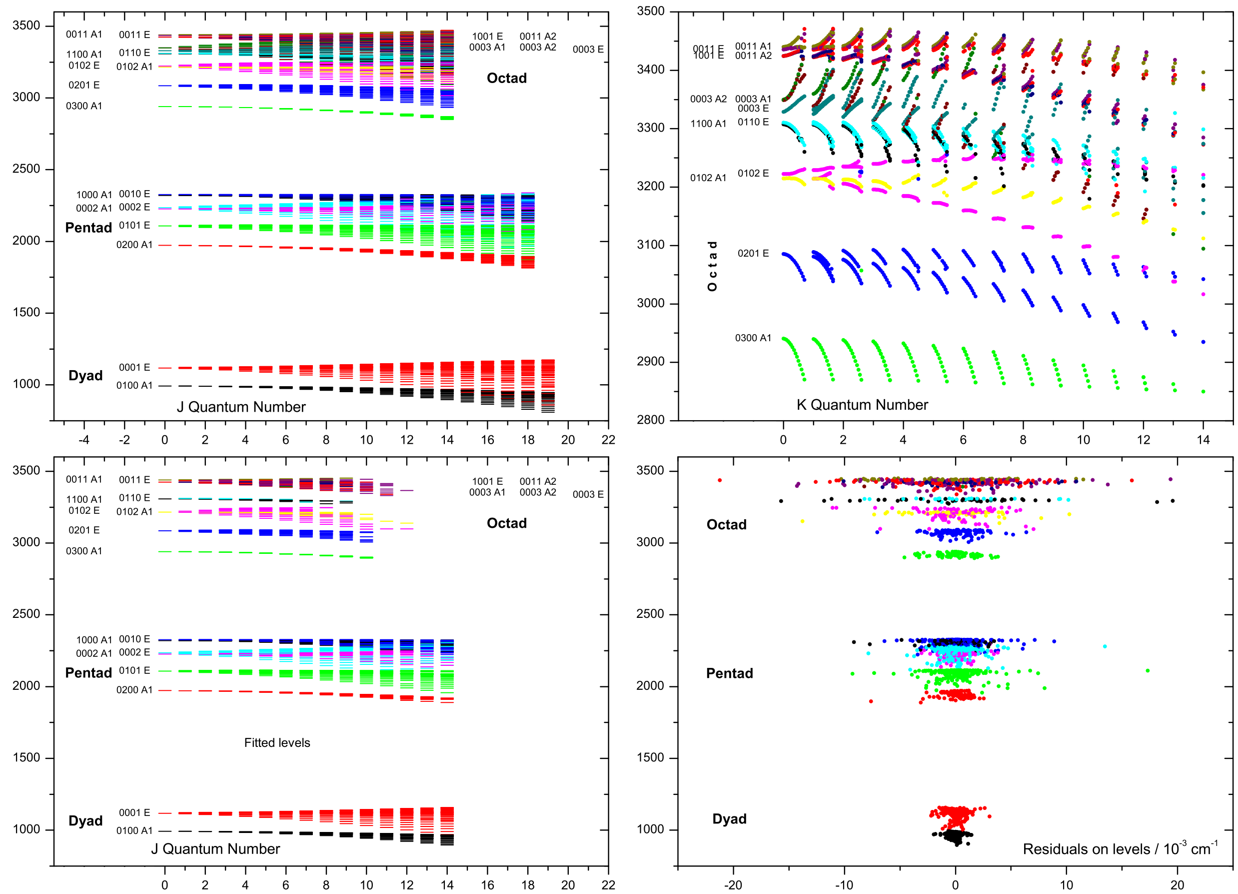

The reduced energies are derived from the ro-vibrational eigenvalues by subtracting the average ground state energy $B"J(J+1)$ with $B"=4.40$ cm^{-1}. The top panels refer to calculated energy levels. The bottom panels refer to fitted levels. The colors of the symbols (web version of this article) are assigned according to the principal vibrational character of the eigenvectors. The color coding can be determined from the $J=0$ levels. The top right panel displays the calculated energies versus the projection quantum number K. At a given K value, the dots representing the associated J levels are shifted horizontally by the quantity $0.05(J-K)$ in order illustrate the behavior of the K series. On the lower part of this panel the $3\nu_2$ upper levels appear displayed along regular paraboloidal branches (as expected for weakly perturbed parallel bands), whereas on the upper part of the panel, several K series present perturbed behaviors reflecting strong ro-vibrational interactions.

Figure 3: Intensity diagrams for the phosphine Pentad and Octad

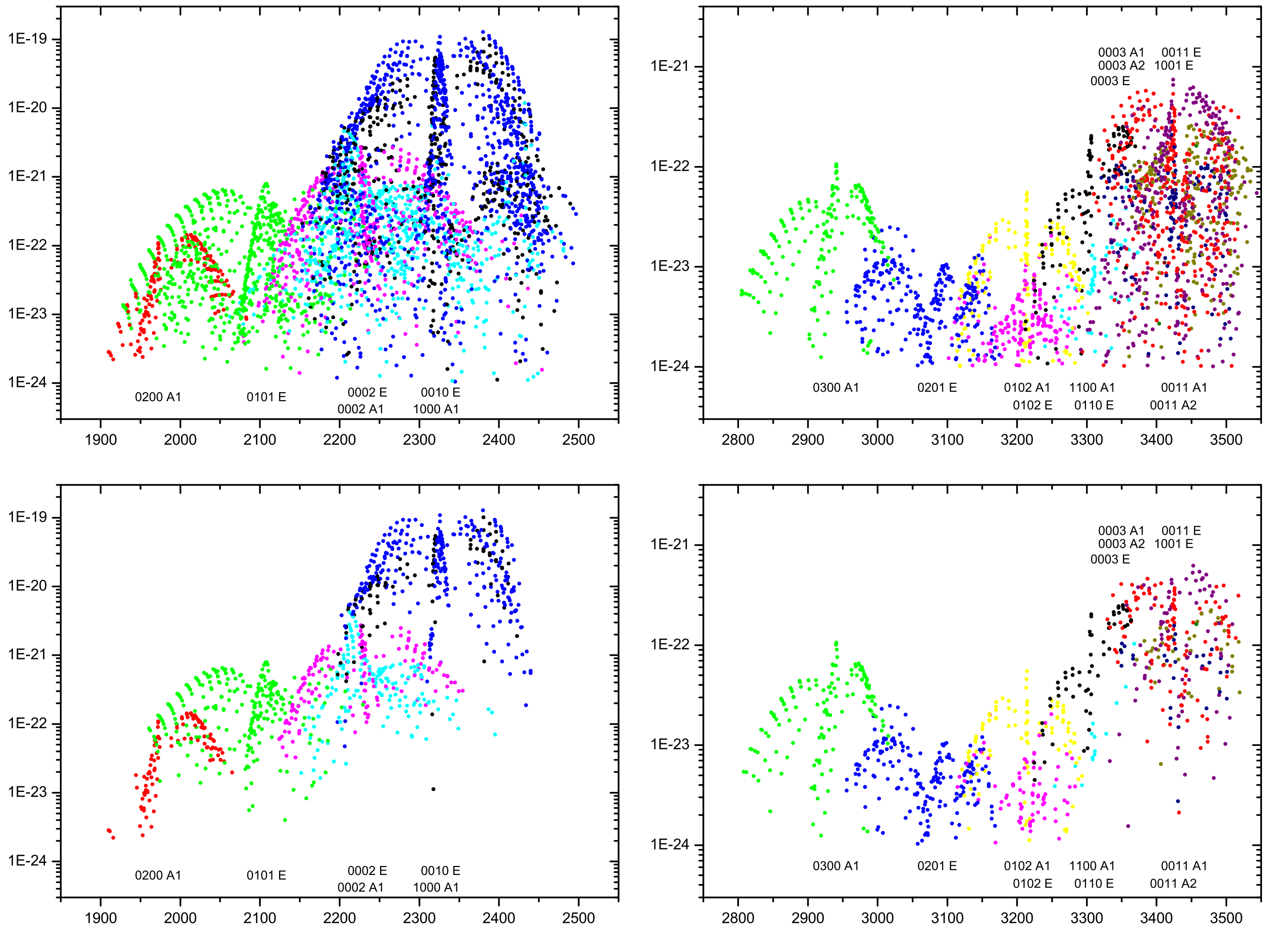

The panels at the top display the intensities of the lines used for fitting the positions for the Pentad and the Octad. The panels at the bottom display the intensities of the lines used for fitting the intensities. These pictures illustrate the order of magnitude coverage of the fitted data for the various bands. The color coding is the same as for the energy diagrams plotted in Fig. 2. For the Pentad, the “observed intensities” shown in the the lower left panel are actually the calculated values from [1].

Table 2: Vibrational energies of the lower three polyads of phosphine

Polyad #	Band	C_{3v} symmetry	Ab initio [19] cm^{-1}	Ab initio [20] cm^{-1}	Present work cm^{-1}	Obs-Calc cm^{-1}	# fitted positions ($J=0$)	(All Js)
1	ν_2	A_1	991.90485	993.00	992.13551	-0.00065	1	
1	ν_4	E	1118.93481	1117.89	1118.30697	-0.00031	1	
2	$2\nu_2$	A_1	1972.383	1974.18	1972.56970	0.00121	1	172
2	$\nu_2+\nu_4$	E	2107.9348	2108.69	2108.15186	-0.00013	1	657
2	$2\nu_4$	A_1	2227.7315	2226.10	2226.83335	0.00176	1	415
2	$2\nu_4$	E	2236.10587	2234.10	2234.92145	-0.00142	1	657
2	ν_1	A_1	2321.042	2322.50	2321.12166	-0.00045	1	454
2	ν_3	E	2325.8028	2326.46	2326.86662	0.00000	1	980
3	$3\nu_2$	A_1	2941.066	2943.06	2940.76667	-0.00006	1	260
3	$2\nu_2+\nu_4$	E	3084.3547	3087.03	3085.65318	-0.00041	1	309
3	$\nu_2+2\nu_4$	A_1	3212.5737	3215.24	3214.93630	-0.00615	1	169
3	$\nu_2+2\nu_4$	E	3221.188	3222.73	3222.50392			223
3	$\nu_1+\nu_2$	A_1	3306.8834	3309.93	3307.56956	- 0.01116	2	108
3	$\nu_2+\nu_3$	E	3311.2245	3312.47	3310.48053			55
3	$3\nu_4$	E	3333.9183	3332.55	3328.82306	(*)		0
3	$3\nu_4$	A_1	3351.0045	3348.51	3348.83292	(*)		1
3	$3\nu_4$	A_2	3350.835	3348.04	3349.82623	(*)		2
3	$\nu_1+\nu_4$	E	3425.48349	3423.80	3424.62191	0.00801	1	367
3	$\nu_3+\nu_4$	A_2	3425.128	3425.08	3424.43377			143
3	$\nu_3+\nu_4$	E	3436.29195	3435.57	3435.61810			389
3	$\nu_3+\nu_4$	A_1	3441.0073	3439.55	3440.25942	-0.00121	1	204

The "Obs-Calc" column refers to vibrational levels ($J = 0$) directly observed in the present work from 1 or 2 transitions. The "# fitted positions" sub-columns distinguish for each band between transitions with $J = 0$ upper level and all J transitions. Empty ($J = 0$) cells indicate that the corresponding vibrational energies are extrapolated from higher J transitions belonging to the corresponding vibrational substates. *Ab initio* values are reproduced with the numbers of digits taken from the original works. (*) Stars emphasize that the $3\nu_4$ subband origins are determined more indirectly through the vibrational hybridization with other observed states. These effective values may have large uncertainties that are difficult to estimate.

Figure 4: MIRS graphical interface

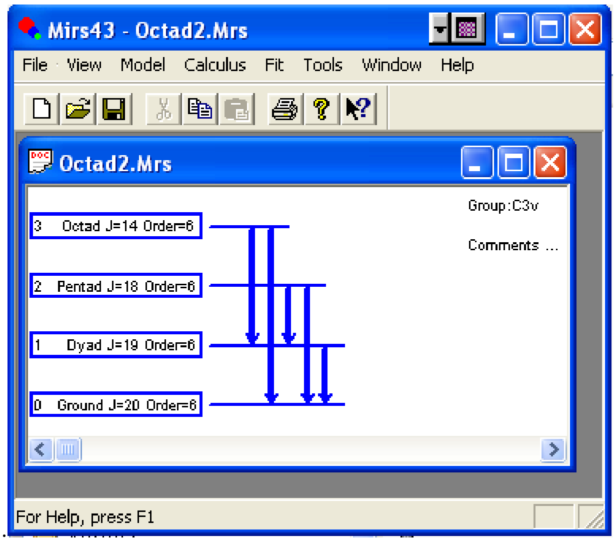

Vertical arrows indicate the band systems involved in the present analysis.

$$\Omega_v = n_1 + n_2 + n_3 + n_4 + m_1 + m_2 + m_3 + m_4. \tag{5}$$

A detailed description of the tensor coupling of elementary operators can be found in Refs. [12, 25].

The effective hamiltonians associated with the subsequent polyads include two, three or four groups of terms obtained by projection of the above hamiltonian operator (3) onto the corresponding subspaces formally denoted by $< Polyad >$:

$$H^{<G.S.>} = H^{<G.S.>}_{\{G.S.\}} \tag{6}$$

$$H^{<Dyad>} = H^{<Dyad>}_{\{G.S.\}} + H^{<Dyad>}_{\{Dyad\}} \tag{7}$$

$$H^{<Pentad>} = H^{<Pentad>}_{\{G.S.\}} + H^{<Pentad>}_{\{Dyad\}} + H^{<Pentad>}_{\{Pentad\}} \tag{8}$$

$$H^{<Octad>} = H^{<Octad>}_{\{G.S.\}} + H^{<Octad>}_{\{Dyad\}} + H^{<Octad>}_{\{Pentad\}} + H^{<Octad>}_{\{Octad\}}. \tag{9}$$

The vibrational states involved in each polyad are listed in Table 2. All the symmetry allowed terms in expansion (3) and their matrix elements in the basis functions are automatically generated by the MIRS computer program [13] in the configuration shown in Fig. 4. In the present study the sixth order of approximation was considered as defined by

$$\Omega_v + \Omega_r - 2. \tag{10}$$

The number of possible and actually adjusted terms involved in each group at each order of expansion is given in Table 3. By comparing with the values for methane given in Table 3 of Ref. [24] one can see that the numbers of symmetry allowed terms are larger for phosphine than for methane at the lower orders and smaller at the higher orders as a consequence of the competition between the total vibrational degrees of freedom and the corresponding degeneracies related to the molecular point groups. For instance, a complete expansion up to the

Table 3: Number of terms in the subsequent groups of the effective hamiltonians for the phosphine molecule

Order	$H_{\{G.S.\}}$	$H_{\{Dyad\}}$	$H_{\{Pentad\}}$	$H_{\{Octad\}}$	$H^{<Octad>}$
0	2 (2)	2 (2)	2 (2)	0	6 (6)
1		2 (2)	6 (2)	0	8 (4)
2	4 (4)	8 (8)	22 (16)	10 (8)	44 (36)
3		6 (5)	34 (26)	36 (13)	76 (44)
4	7 (5)	18 (17)	72 (43)	107 (52)	207 (117)
5		12 (8)	86 (23)	180 (56)	278 (87)
6	10 (7)	32 (25)	152 (32)	329 (54)	523 (118)
Total	23 (18)	80 (67)	374 (144)	662 (183)	1139 (412)

The number of non-zero parameters (fixed or adjusted) are quoted in parentheses. According to the vibrational extrapolation scheme, the columns "$H_{\{Polyad\}}$" refer to terms belonging to specified polyads. The last column "$H^{<Octad>}$" summarizes the terms at each order in the projection of the global hamiltonian onto the Octad band system according to Eq. (9).

fifth order contains respectively 616 and 870 terms for the phosphine and the methane molecules.

Within the polyad scheme defined by Eq. (3), there are four first order vibrationally off-diagonal coupling terms (two Coriolis and two Fermi). The Coriolis term $T^{1(1,1E)}_{0100,0001}$ appears first in the Dyad as the dominant interaction between ν_2 and ν_4. It has non-vanishing off-diagonal matrix elements connecting several substates among the Pentad and Octad. The Coriolis term $T^{1(1,1E)}_{1000,0010}$ coupling ν_1 and ν_3 appears first in the Pentad. Similarly the Fermi terms $T^{0(0,0A_1)}_{1000,0200}$ and $T^{0(0,0A_1)}_{1000,0002}$ appear first in the Pentad. They have non-vanishing matrix elements within the Octad. According to the concept of vibrational extrapolation, in our global model these four terms are adjusted by fitting simultaneously all available experimental data involved in the three polyads considered. This also apply more generally to all other and higher order terms ensuring a consistent propagation of experimental information into an optimized and unique set of effective hamiltonian parameters. Of course not all the 1139 effective hamiltonian terms can be adjusted simultaneously. The main reason is that, given a set of hamiltonian eigenvalues, there exist in principle an infinite number of equivalent sets of effective parameters corresponding to various forms of reduced hamiltonians [31]. This is already true for isolated band models and more pronounced in the case of a polyad adapted model. The theory of reduced hamiltonians is particularly hard to manage in the case of complex systems like the one considered in the present work. We had to rely on a more pragmatical approach by considering the statistical correlations at each stage of the iterative numerical least squares procedure. It is however noteworthy that the global analysis based on the hamiltonian form given in Eq. (3) optimizes the decorrelation among the adjusted parameters. The numbers and types of parameters are summarized in Table 4.Our model includes 412 effective parameters. 248 are vibrationally diagonal terms and 165 vibrationally off-diagonal terms.

The dipolar transition moment was similarly expressed in tensorial form. It is partially transformed following the polyad pattern of the PH_3 molecule. According to our unified treatment of both energies and intensities, this transformation is *de facto* fully consistent with the transformation of the hamiltonian itself. In the present paper, three sets of effective dipole moment parameters were considered to describe the intensities of the $\Delta n = 1$, $\Delta n = 2$ and $\Delta n = 3$ band systemswhere n is the polyad number defined by Eq. (2).

Table 4: Summary of the hamiltonian parameters for the ground state, Dyad, Pentad and Octad of PH_3

Nb	Ω_{max}	ΔK_{max}	(Coupled) States	Type	Polyad (Band)
18	8	6	0000	diagonal	Ground State
10	6	3	0100	diagonal	Dyad (ν_2)
24	6	5	0100 | 0001	off-diagonal	Dyad (ν_2 / ν_4)
33	6	6	0001	diagonal	Dyad (ν_4)
11	6	3	1000	diagonal	Pentad (ν_1)
2	2	2	1000 | 0101	off-diagonal	Pentad (ν_1 / $\nu_2+\nu_4$)
24	6	5	1000 | 0010	off-diagonal	Pentad (ν_1 / ν_3)
16	4	4	1000 | 0002	off-diagonal	Pentad (ν_1 / $2\nu_4$)
3	2	0	0200	diagonal	Pentad ($2\nu_2$)
2	2	2	0200 | 0101	off-diagonal	Pentad ($2\nu_2$ / $\nu_2+\nu_4$)
1	2	2	0200 | 0010	off-diagonal	Pentad ($2\nu_2$ / ν_3)
1	2	2	0200 | 0002	off-diagonal	Pentad ($2\nu_2$ / $2\nu_4$)
12	4	4	0101	diagonal	Pentad ($\nu_2+\nu_4$)
4	2	2	0101 | 0010	off-diagonal	Pentad ($\nu_2+\nu_4$ / ν_3)
9	2	2	0101 | 0002	off-diagonal	Pentad ($\nu_2+\nu_4$ / $2\nu_4$)
37	6	6	0010	diagonal	Pentad (ν_3)
6	2	2	0010 | 0002	off-diagonal	Pentad (ν_3 / $2\nu_4$)
16	3	2	0002	diagonal	Pentad ($2\nu_4$)
4	4	0	1100	diagonal	Octad ($\nu_1+\nu_2$)
4	3	2	1100 | 1001	off-diagonal	Octad ($\nu_1+\nu_2$ / $\nu_1+\nu_4$)
4	3	2	1100 | 0110	off-diagonal	Octad ($\nu_1+\nu_2$ / $\nu_2+\nu_3$)
4	3	2	1100 | 0102	off-diagonal	Octad ($\nu_1+\nu_2$ / $\nu_2+2\nu_4$)
3	2	2	1100 | 0011	off-diagonal	Octad ($\nu_1+\nu_2$ / $\nu_3+\nu_4$)
1	1	1	1100 | 0003	off-diagonal	Octad ($\nu_1+\nu_2$ / $3\nu_4$)
15	4	4	1001	diagonal	Octad ($\nu_1+\nu_4$)
12	3	3	1001 | 0110	off-diagonal	Octad ($\nu_1+\nu_4$ / $\nu_2+\nu_3$)
24	3	3	1001 | 0011	off-diagonal	Octad ($\nu_1+\nu_4$ / $\nu_3+\nu_4$)
1	1	1	1001 | 0003	off-diagonal	Octad ($\nu_1+\nu_4$ / $3\nu_4$)
3	2	0	0300	diagonal	Octad ($3\nu_2$)
6	2	2	0201	diagonal	Octad ($2\nu_2+\nu_4$)
5	2	2	0201 | 0102	off-diagonal	Octad ($2\nu_2+\nu_4$ / $\nu_2+2\nu_4$)
9	3	3	0110	diagonal	Octad ($\nu_2+\nu_3$)
3	2	2	0110 | 0102	off-diagonal	Octad ($\nu_2+\nu_3$ / $\nu_2+2\nu_4$)
7	2	2	0110 | 0011	off-diagonal	Octad ($\nu_2+\nu_3$ / $\nu_3+\nu_4$)
7	2	2	0110 | 0003	off-diagonal	Octad ($\nu_2+\nu_3$ / $3\nu_4$)
9	2	2	0102	diagonal	Octad ($\nu_2+2\nu_4$)
1	0	0	0102 | 0011	off-diagonal	Octad ($\nu_2+2\nu_4$ / $\nu_3+\nu_4$)
52	4	4	0011	diagonal	Octad ($\nu_3+\nu_4$)
10	2	2	0003	diagonal	Octad ($3\nu_4$)

Ω_{max} and ΔK_{max} designate respectively the maximum J power with respect to the angular momentum components J_α and the maximum value of ΔK for matrix elements in each category. The complete list of hamiltonian parameters is available from the separate file `Hamiltonian_parameters.txt` .

The first set led to the Pentad−Dyad effective dipole expansion formally expressed as

$$\mu^{<Pentad-Dyad>} = \mu^{<Pentad-Dyad>}_{\{Dyad-G.S.\}} + \mu^{<Pentad-Dyad>}_{\{Pentad-Dyad\}}, \tag{11}$$

where the first term gathers operators involved in transitions from the ground state to the Dyad and the second group contains additional higher order operators contributing to transitions from the Dyad to the Pentad only.

The second set led to the Pentad and Octad−Dyad effective dipole expansions as

$$\mu^{<Pentad-G.S.>} = \mu^{<Pentad-G.S>}_{\{Pentad-G.S.\}} \tag{12}$$

and

$$\mu^{<Octad-Dyad>} = \mu^{<Octad-Dyad>}_{\{Pentad-G.S.\}} + \mu^{<Octad-Dyad>}_{\{Octad-Dyad\}}. \tag{13}$$

The interpretation of the two groups in Eq. (13) can be simply deduced from the one of the first set by shifting the polyad numbers by 1.

The third set constituted the Octad effective dipole expansion as

$$\mu^{<Octad-G.S.>} = \mu^{<Octad-G.S>}_{\{Octad-G.S.\}}. \tag{14}$$

These parameter sets were used to predict intensities of the three polyads and of the hot bands arising from the Dyad. To describe the intensities of the cold Octad band system (3 μm region) a set of 38 effective dipole moment parameters has been used including terms up to the third order of approximation among the 66 symmetry allowed terms at that order. The list is available from the separate file `Octad_dipole_moment.txt`.

4 Results and discussion

A great majority of the experimental data fitted in the present work were already assigned and fitted in previous works [1, 3, 7]. However, as mentioned earlier, the transfer of these assignments in our model could not be done in a fully automatic way on the basis of the usual approximate quantum numbers. As a matter of fact, since our model is designed to account explicitly for strong interactions, the assignment is primarily based on quantum numbers associated to fundamental invariants, namely the angular momentum J and the ro-vibrational symmetry C in the C_{3v} molecular point group. By construction the polyad number n is also a robust pseudo quantum number. It is not always true for the usual quantum numbers related to the harmonic oscillator and rigid rotor approximation, namely the v_i's (principal vibrational quantum numbers) and K (projection of the angular momentum along the molecular axis). These approximate quantum numbers are not explicitly taken into account into our assignment procedure. Instead the running number α of the hamiltonian eigenvalues within a given n, J, C matrix-block is used. Note that the α assignment is not robust either. In the case of heavily mixed ro-vibrational states, α may vary as the effective hamiltonian parameters in the course of the iterative non-linear least squares procedure. For these reasons at various stages of the analysis a careful “by hand” inspection of the system had to be done. A few (if not to say one) missagnments can have nasty effects on many other levels. Conversely it is well known that heavily intricate levels give more information than non perturbed

Table 5: Summary of results for bands in the PH_3 Pentad

Band	# Calc lines	Fmin cm^{-1}	Fmax cm^{-1}	# Fitted Positions	St.Dev. 10^{-3} cm^{-1}	# Fitted Intensities	Int. Sum / cm^{-2} atm^{-1} Present	*Ab initio* [21]
$2\nu_2(A_1)$	1102	1725.	2127.	172	1.1	108	0.27	0.0947
$2\nu_4(A_1)$	2528	2047.	2549.	415	1.1	158	6.2	6.7036
$\nu_1(A_1)$	2946	2064.	2561.	454	1.7	103	137	112.9179
$\nu_2+\nu_4(E)$	3273	1856.	2345.	657	1.8	255	2.7	1.6058
$2\nu_4(E)$	4399	1930.	2571.	657	1.5	162	12	4.1623
$\nu_3(E)$	5472	2075.	2577.	980	1.8	299	367	444.6091

The present intensity summations are indicative only. *Ab initio* values are reproduced with the numbers of digits taken from the original works.

Table 6: Summary of results for hot bands in the PH_3 Pentad–Dyad system

Band	# Calc lines	Fmin cm^{-1}	Fmax cm^{-1}	# Fitted Positions	St.Dev. 10^{-3} cm^{-1}	Int. Sum / cm^{-2} atm^{-1} Present	*Ab initio* [21]
$2\nu_2(A_1)$ - $\nu_2(A_1)$	632	792.	1132.	0	-	1.1	1.1198
$2\nu_4(A_1)$ - $\nu_4(E)$	1287	903.	1321.	11	1.0	0.34	0.3780
$\nu_2+\nu_4(E)$ - $\nu_2(A_1)$	1566	897.	1315.	21	1.2	0.59	0.7256
$\nu_2+\nu_4(E)$ - $\nu_4(E)$	1629	816.	1149.	15	0.8	0.68	0.6452
$2\nu_4(E)$ - $\nu_4(E)$	1860	855.	1329.	21	1.0	0.61	-
$2\nu_4(A_1)$ - $\nu_2(A_1)$	95	1231.	1362.	0	-	0.001	0.0058
$2\nu_2(A_1)$ - $\nu_4(E)$	20	842.	980.	0	-	0.0002	-
$\nu_3(E)$ - $\nu_4(E)$	277	1001.	1306.	0	-	0.011	-
$2\nu_4(E)$ - $\nu_2(A_1)$	28	1033.	1303.	0	-	0.001	-
$\nu_1(A_1)$ - $\nu_4(E)$	81	1003.	1306.	0	-	0.002	-

The present intensity summations are indicative only. *Ab initio* values are reproduced with the numbers of digits taken from the original works.

levels. It should be emphasized that thanks to the vibrational extrapolation scheme implemented in our global model (as outlined in section 3 about the off-diagonal Coriolis and Fermi terms), the dominant interactions which generally affect the system from the lower polyads upwards are constrained by the observations on the lower polyads. They are *de facto* involved in the higher polyad description, and only weaker interactions or vibrational corrections of the previous ones need to be adjusted to the higher polyad observations.

In the present work, the so-called ground-state parameters (from $H_{\{G.S.\}}$) involved in all effective hamiltonians of the three upper polyads according to Eqs. 6 to 9, were kept fixed throughout at the values of [2]. All other 395 parameters were adjusted to fit simultaneously the ”observed” upper energy levels of the Dyad [3], the measured transition wavenumbers of the Pentad [1], the measured transition wavenumbers of the Octad [7] and newly assigned transition wavenumbers from the Octad as well as from the Octad–Dyad and Pentad–Dyad band systems.The whole set of 412 terms have non-vanishing matrix elements within the Octad system. Among them the 180 “Octad” terms listed at the bottom part of Table 4 have vanishing matrix elements within the lower polyads and most of them can be considered as vibrational corrections of terms already involved in the Dyad and Pentad. For comparison, 150 parameters were introduced in the isolated band model used in Ref. [7] to assign the transitions from 7 of the 8 bands involved in the Octad. Our 180 “Octad” terms represent only a slightly larger set of parameters, but they are capable of modeling all the bands by considering all relevant interactions as shown hereafter.

Table 7: Summary of results for bands in the PH_3 Octad

Band	# Calc lines	Fmin cm^{-1}	Fmax cm^{-1}	Nb Fitted Positions	St. Dev. 10^{-3} cm^{-1}	# Fitted Intensities	Int. Sum / cm^{-2} atm^{-1} Present	*Ab initio* [21]
$3\nu_2(A_1)$	562	2733.	3177.	260	1.9	182	0.17	0.2052
$\nu_2+2\nu_4(A_1)$	419	3074.	3392.	169	3.2	111	0.066	0.0956
$\nu_1+\nu_2(A_1)$	1035	3083.	3438.	108	6.7	58	0.44	0.2878
$3\nu_4(A_1)$	770	3100.	3606.	1	8.2	0	0.073	
$\nu_3+\nu_4(A_1)$	1790	3242.	3639.	204	5.0	41	0.81	0.8801
$2\nu_2+\nu_4(E)$	926	2900.	3436.	309	2.0	201	0.061	0.0489
$\nu_2+2\nu_4(E)$	1072	2935.	3448.	223	2.7	82	0.046	0.0346
$\nu_2+\nu_3(E)$	2024	3106.	3508.	55	4.7	14	0.22	0.0542
$\nu_1+\nu_4(E)$	2678	3095.	3636.	367	5.4	117	1.7	
$\nu_3+\nu_4(E)$	2726	3227.	3638.	389	5.3	82	1.7	0.0067
$\nu_3+\nu_4(A_2)$	1305	3208.	3629.	143	4.3	30	0.44	3.5448
$3\nu_4(E)$	1171	3103.	3594.	0	-	0	0.093	0.0073
$3\nu_4(A_2)$	565	3132.	3619.	2	0.6	1.9	0.054	

The present intensity summations are indicative only. *Ab initio* values are reproduced with the numbers of digits taken from the original works.

Table 8: Summary of results for hot bands in the PH_3 Octad−Dyad system

Band	# Calc lines	Fmin cm^{-1}	Fmax cm^{-1}	# Fitted Positions	St.Dev. 10^{-3} cm^{-1}	Int. Sum / cm^{-2} atm^{-1} Present	*Ab initio* [21]
$3\nu_2(A_1)$ - $\nu_2(A_1)$	192	1901.	2050.	0	-	0.006	0.0004
$\nu_2+2\nu_4(A_1)$ - $\nu_2(A_1)$	520	2107.	2434.	4	0.6	0.049	0.0441
$\nu_2+2\nu_4(A_1)$ - $\nu_4(E)$	258	1937.	2299.	0	-	0.007	0.0072
$\nu_1+\nu_2(A_1)$ - $\nu_2(A_1)$	1332	2121.	2478.	34	4.2	1.1	0.9390
$\nu_1+\nu_2(A_1)$ - $\nu_4(E)$	553	2025.	2410.	0	-	0.017	-
$3\nu_4(A_1)$ - $\nu_4(E)$	974	2118.	2505.	0	-	0.071	0.0402
$\nu_3+\nu_4(A_1)$ - $\nu_2(A_1)$	439	2303.	2619.	0	-	0.015	-
$\nu_3+\nu_4(A_1)$ - $\nu_4(E)$	2524	2122.	2565.	50	4.5	0.86	1.0173
$3\nu_4(A_2)$ - $\nu_4(E)$	799	2131.	2484.	0	-	0.064	0.0296
$\nu_3+\nu_4(A_2)$ - $\nu_4(E)$	1981	2082.	2555.	25	3.7	1.0	1.0123
$2\nu_2+\nu_4(E)$ - $\nu_2(A_1)$	635	1921.	2444.	10	1.6	0.037	0.0248
$\nu_2+2\nu_4(E)$ - $\nu_2(A_1)$	1297	2110.	2461.	0	-	0.098	0.0308
$\nu_2+2\nu_4(E)$ - $\nu_4(E)$	589	1934.	2383.	2	2.1	0.022	-
$\nu_2+\nu_3(E)$ - $\nu_2(A_1)$	2345	2137.	2523.	18	2.0	3.2	3.6638
$3\nu_4(E)$ - $\nu_2(A_1)$	1280	2113.	2571.	1	2.9	0.18	0.0215
$3\nu_4(E)$ - $\nu_4(E)$	1750	2070.	2473.	0	-	0.13	0.1533
$\nu_1+\nu_4(E)$ - $\nu_4(E)$	3845	2052.	2536.	30	5.8	1.15	0.8342
$\nu_3+\nu_4(E)$ - $\nu_4(E)$	4066	2082.	2555.	41	4.8	1.6	0.4335
$\nu_1+\nu_4(E)$ - $\nu_2(A_1)$	1112	2118.	2608.	0	-	0.073	-
$2\nu_2+\nu_4(E)$ - $\nu_4(E)$	102	1959.	2272.	0	-	0.001	-
$\nu_2+\nu_3(E)$ - $\nu_4(E)$	958	2024.	2464.	0	-	0.044	-
$\nu_3+\nu_4(A_2)$ - $\nu_2(A_1)$	496	2289.	2598.	0	-	0.024	0.0047
$3\nu_4(A_1)$ - $\nu_2(A_1)$	429	2110.	2576.	0	-	0.039	-
$\nu_3+\nu_4(E)$ - $\nu_2(A_1)$	868	2235.	2622.	0	-	0.032	-
$3\nu_4(A_2)$ - $\nu_2(A_1)$	134	2128.	2590.	0	-	0.020	-

The present intensity summations are indicative only. *Ab initio* values are reproduced with the numbers of digits taken from the original works.

At the final stage of our fitting procedure, 2245 levels (up to $J = 14$) observed through more than 6000 transitions arising from 34 cold and hot bands including all available experimental data have been fitted simultaneously using a unique set of effective hamiltonian parameters (lower left panel of Fig. 2). The complete list of these parameters is available from the separate file `Hamiltonian_parameters.txt` or by request to the authors. The list includes for each parameter the tensor nomenclature as given by Eq. (4), the untruncated input values to the MIRS program, the rounded value and the corresponding standard deviation. As mentioned already in section 3, the selection of the parameters and thus the reduced form of the hamiltonian were done pragmatically on the basis of the statistical standard deviations and correlations of the parameters. A comparison with parameters reported in previous works would not be meaningful unless the respective reduced forms are taken into account. This would require too complex theoretical calculations especially for relating isolated to interacting band models for the Octad. The total number of effective hamiltonian parameters determined in the present work might appear rather large. In fact standard ratios indicate that the number of adjusted parameters is actually optimized with respect to previous works. For instance the ratio of the number of observed data over the number of adjusted parameters is larger than 16. On average, our model includes less than 7 parameters per band.

The rms achieved is 0.63×10^{-3} cm^{-1} for 472 Dyad levels ; 1.5×10^{-3} cm^{-1} for 3332 Pentad transitions and 4.3×10^{-3} cm^{-1} for 2579 Octad transitions. Detailed statistics giving the number of data fitted for each band are reported in Tables 5, 6, 7 and 8.The intensity diagrams plotted in Fig. 3 give a graphical overview of the actual coverage of the fitted data for positions (top panels) and for intensities (bottom panels). They show the importance of having data with intensities covering several orders of magnitude and conversely they give a feeling of the difficulty of retrieving accurate measurements in such congested spectra. The lower right panel of Fig. 2 displays the distribution of the position residuals over the various bands of the system. It should be emphasized that the assignment and fitting process were guided by a systematic selection of the levels involved in multiple transition observations through a generalization of the well proven method of combination differences. Many other transitions than those quoted in the Tables can in fact be unambiguously assigned. Such straightforward assignments would not provide significantly independent information. The precision achieved on the Dyad is quite similar to the one of the previous work of Ref. [3]. The Pentad region around 4.5 μm were fairly well reproduced thanks to assigned data distributed over all the six substates of the polyad (Table 5). Several hot band transitions arising from both ν_2 and ν_4 upper states were also included (Table 6). The present work improves the modeling of the Pentad upper states by dividing the rms reported in the previous work of Ref. [1] by a factor 6. Since essentially the same data were used in both works, the main explanation for this is the efficiency of our present model and the flexibility of its computer implementation in modeling intra-polyad interactions. Finally, in the 3 μm region the present work represents the first high-resolution modeling with a standard deviation not far from the experimental precision. A qualitative picture of the improvement achieved on the Octad is illustrated in Fig. 5 on the basis of the assignments reported in [7]. In this diagram, the size of the symbols reflect the order of magnitude of the discrepancies between the isolated band models used in [7] and the present polyad model. Using the present model, the rms (Obs-Calc) on the 593 levels in common with both works is 3.6×10^{-3} cm^{-1}, whereas the discrepancies using isolated band models reach rather high values : 282 are larger than 10^{-2} cm^{-1}; 82 are larger than 10^{-1} cm^{-1} and 40 exceed 1 cm^{-1}. As expected the most

Table 9: Sample fitting of ν_2, $2\nu_4$ and $3\nu_2$

Position (cm^{-1})	Obs - Calc (10^{-3} cm^{-1})	Intensity (cm / molecule)	(O - C) / Calc %	Vibrational	Rotational
911.91440	-0.4	0.627E-20	-6.5	$\nu_2(A_1)$	$^QP(8,0,A1)$
2164.03828	0.2	0.645E-21	-2.6	$2\nu_4(A_1)$	$^QP(8,0,A1)$
2847.41733	0.8	0.212E-22	1.5	$3\nu_2(A_1)$	$^QP(8,0,A1)$
901.38211	-0.3	0.419E-20	-7.5	$\nu_2(A_1)$	$^QP(9,2,E)$
2155.29851	-0.2	0.473E-21	-4.7	$2\nu_4(A_1)$	$^QP(9,2,E)$
2834.31465	0.6	0.141E-22	-1.1	$3\nu_2(A_1)$	$^QP(9,2,E)$
900.42341	0.3	0.117E-20	-4.2	$\nu_2(A_1)$	$^QP(10,8,E)$
2142.98756	0.4	0.161E-21	-5.9	$2\nu_4(A_1)$	$^QP(10,8,E)$
2845.70393	-0.9	0.562E-23	2.5	$3\nu_2(A_1)$	$^QP(10,8,E)$

Each of the three groups involves three transitions with common lower states, common rotational selection rules and upper states belonging to the Dyad, Pentad and Octad.

significant improvements are obtained in the complex upper part of the Octad. The modeling of the transition intensities based on consistent sets of effective dipole moment operators for cold and hot bands (presented in section 3) has been simultaneously undertaken for direct comparison between observed and modeled absorption from 700 to 3500 cm^{-1}. The preliminary results are reported here in terms of integrated band strengths along with the corresponding values recently predicted from *ab initio* calculations [21] (last column in Tables 5, 6, 7 and 8).

A complete line list covering the region from 700 to 3500 cm^{-1} is available from the separate file `Line_List_296K.txt`. It includes all calculated transitions belonging to the 34 different cold and hot bands (Tables 5, 6, 7 and 8) with intensities at 296 K above the threshold of 10^{-24} cm$\times$molecule^{-1}. The list includes the calculated wavenumbers and intensities at 296 K, the corresponding residuals for the data included in the global fit and the vibrational and rotational assignments according to the conventional nomenclature. As mentioned previously, this nomenclature uses approximate quantum numbers that are not always meaningful. They were assigned in the present work on the basis of the eigenvector analysis. Doing so the quoted quantum numbers reflect the dominant basis function component of the eigenfunctions. In particular, the dominant vibrational character is used in the color coding of the energy diagrams plotted in Figs. 2, 3 and 5. The format of the list is similar to the one of Tables 9 and 10. The former shows sample fitted transitions belonging to the Dyad, Pentad and Octad. The later, in the appendix, lists transitions in the range from 3420 to 3430 cm^{-1}. A plot in the same region of the simulated and experimental spectra is represented in the bottom right panel of Fig. 6 . Similar sample plots under the same experimental conditions around the other band origins of the Octad are represented in the other panels of Fig. 6. The simulations were performed using a standard Voigt line profile under a pressure of 6.3 torr, a path length of 16.25 m and a temperature of 289 K. For clarity, the experimental spectrum (lower trace) was re-scaled in such a way that the corrected baseline come close to an horizontal straight line. Due to saturation effects the observed absorption peaks do not reflect precisely the observed intensities. *T*he $3\nu_2$ band is weakly perturbed and was already well described using an isolated band model (Fig. 5). For the higher energy bands where the perturbations are much larger, the agreement between the experimental and the synthetic spectra are globally satisfying, although in some places predicted weak features do not fit very well with the experiments.

Figure 5: Diagram of reduced energy Octad levels involved in both isolated and polyad models

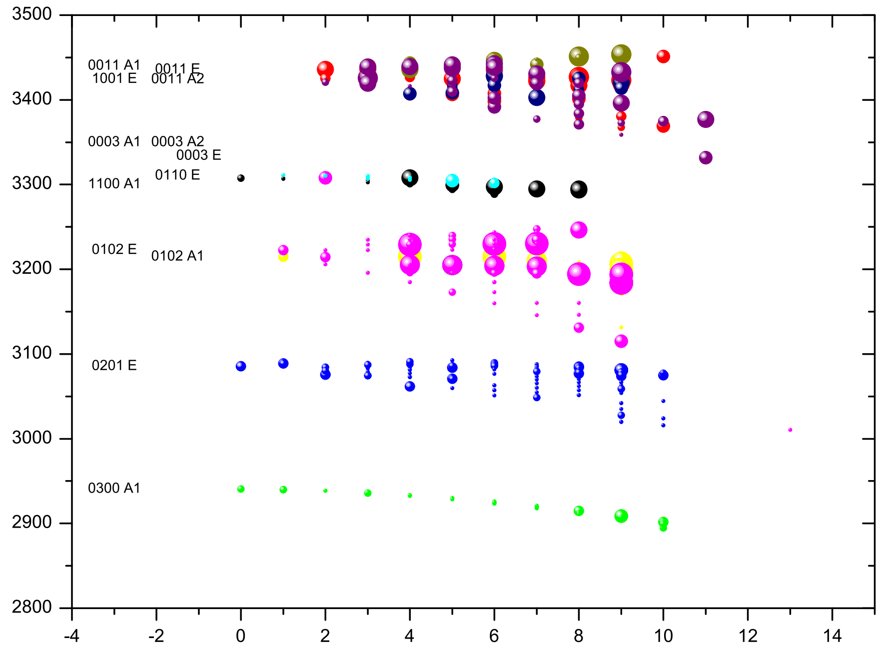

This diagram includes the 593 fitted Octad upper levels that were already assigned in [7]. The color convention is the same as in Figs. 2 and 3. The size of the symbols reflects the order of magnitude of the differences "isolated versus polyad" residuals (see text).

Such discrepancies like the ones around the $\nu_2 + \nu_3$ band origin near 3310 cm^{-1} are believed to arise essentially from inaccuracies in the intensity modeling in progress.

The top right panel of Fig. 2 displays the calculated energies versus the projection quantum number K. At a given K value, the dots representing the associated J levels are shifted horizontally by the quantity $0.05(J - K)$ in order illustrate the behaviour of the K series. On the lower part of this panel the $3\nu_2$ upper levels appear displayed along regular paraboloidal branches (as expected for weakly perturbed parallel bands), whereas on the upper part of the panel, several K series present perturbed behaviours reflecting strong ro-vibrational interactions. Also in this picture, the colors of a few dots and thus the corresponding vibrational assignments might appear anomalous. It illustrates in fact situations where the eigenvector leading coefficients are somewhat unstable.

The main remaining difficulty is for the $3\nu_4$ band and to a lesser extend for $\nu_2 + \nu_3$. These relatively weak bands with three and two quanta respectively are located in a very crowded region and a higher experimental resolution would certainly be helpful. Practically all the $\nu_2 + \nu_3$ lines are very weak and the number of combination differences is not large enough to eliminate wrong assignments. Assigning the $\nu_2 + \nu_3 - \nu_2$ hot band could certainly be useful. This task is not simple since it requires the simultaneous assignment of high J transitions. The statistics shown in Table 7 report only one transition for the A_1 substate of $3\nu_4$ and two for the A_2 substate.

Figure 6: Sample spectra of phosphine around the Octad band origins

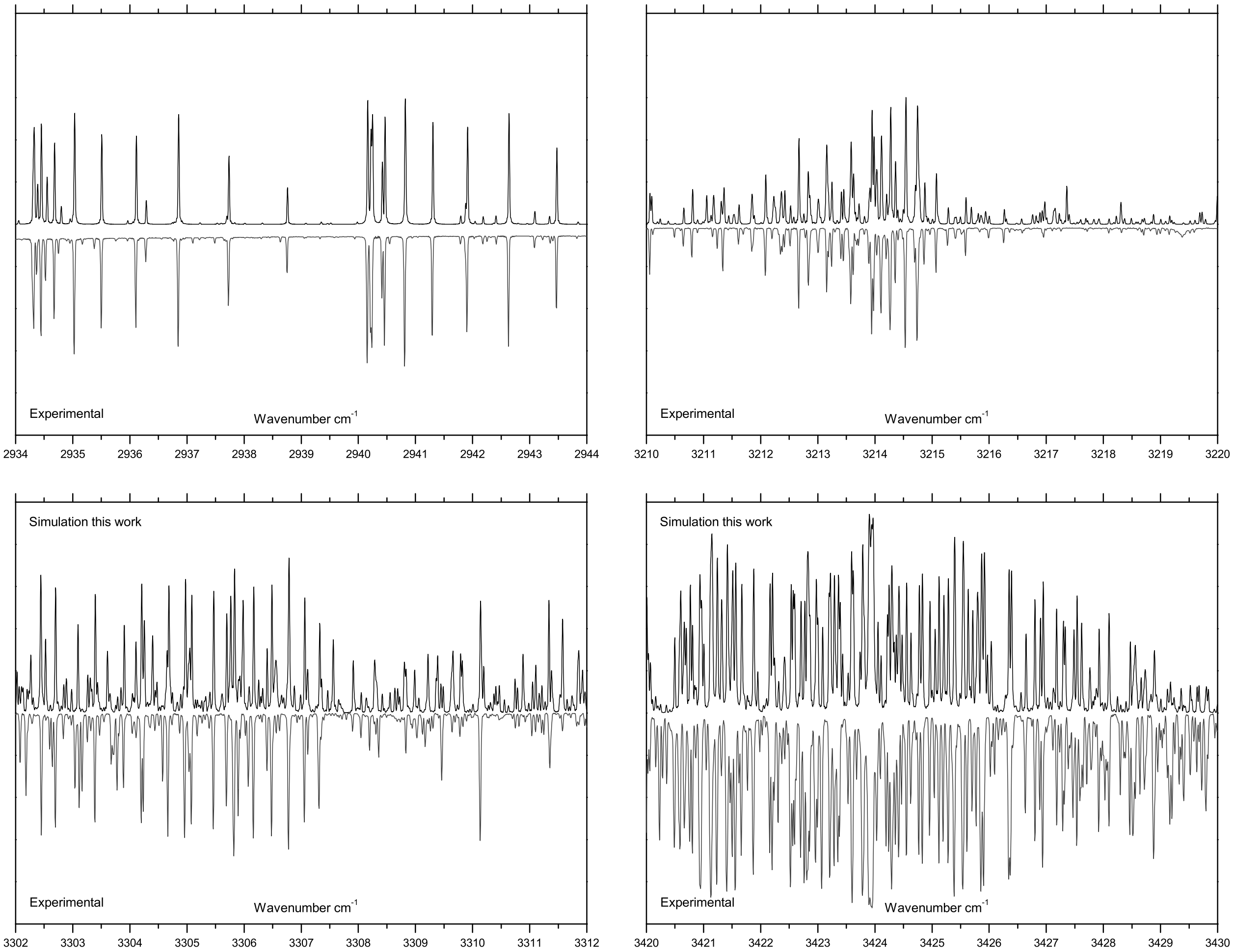

The experimental trace (at the bottom) was recorded using the Kitt Peak FTS at 0.0115 cm-1 resolution with a path length of 16.25 m and a pressure of 6.3 torr at 289 K. The simulated trace (at the top) was calculated using a Voigt line profile under the same experimental conditions. From left to right and from top to bottom the panels correspond to spectral regions around the $3\nu_2$, $\nu_2 + 2\nu_4$, $\nu_1 + \nu_2/\ \nu_2 + \nu_3$ and $\nu_3 + \nu_4/\ \nu_1 + \nu_4$ band origins respectively.

Figure 7: Absorption contribution from the hot bands in the PH_3 Pentad−Dyad and Octad−Dyad systems

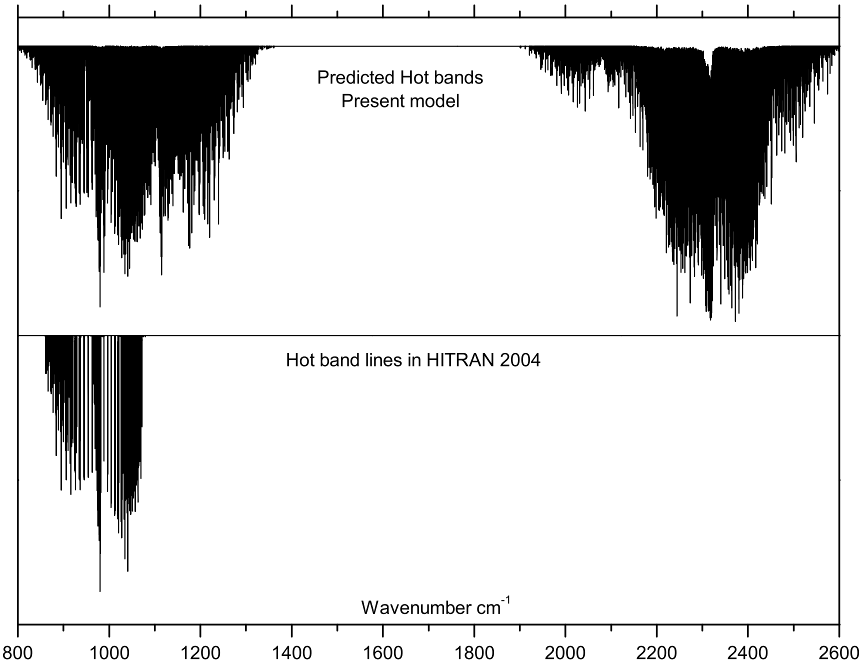

The trace at the top includes all the Pentad−Dyad and Octad−Dyad transitions predicted by the present global model. The bottom trace includes all hot band lines available from the HITRAN database [8]. Both simulations were performed using the same Voigt line profile under the same experimental conditions (pressure 6.3 torr ; path length 4.25 m ; temperature 289 K).

This may be considered as inconsistent with the presence of as many as ten vibrationally diagonal parameters directly related to $3\nu_4$ as quoted in the bottom raw of Table 4. In fact, due to the vibrational hybridization induced by interactions, several other transitions carry a non leading $3\nu_4$ character and thus contribute to the determination of the above parameters.

An important improvement of the present study with respect to previous works lies in its exhaustivity. Even though the precision of the empirical wavenumbers and intensities [7] of the stronger and well resolved spectral features is better than the average precision of the present calculated line parameters, the completeness of the theoretical calculation is essential for planetary applications. Fig. 7 shows an overview of the hot band contributions arising from the 0100 and 0001 states in the 800 to 2600 cm^{-1} region at room temperature. The trace at the top includes all the Pentad−Dyad and Octad−Dyad transitions predicted from the present global model. The trace at the bottom shows all hot band lines available in the HITRAN database [8]. The HITRAN compilation is actually restricted to some of the lines arising from the 0100 state. Note that many of the hot band transitions were fitted in the present global analysis. All these lines are included in the complete line list available from the separate file `Line_List_296K.txt`.

The comparison of the band origins derived from the present ro-vibrational analysis with the values calculated independently from recent *ab initio* studies shows a fairly good agreement of about one reciprocal centimeter rms. The largest discrepancies are observed for the $3\nu_4$ band and especially for the $3\nu_4(E)$ sub-band. The precision of our predictions is believed to be much less than for the other bands due to the very small number of assigned transitions related to the $3\nu_4$ band. The comparison of the integrated band intensities quoted in Tables 5, 6, 7 and 8 shows fairly good coincidences and large discrepancies as well. Before drawing definite conclusions, it should be kept in mind that our intensity analysis is only a preliminary semi-quantitative study. Furthermore, for strongly interacting bands the partial summations may be no longer fully meaningful and thus no longer comparable directly.

At the onset of this project, we expected to locate the hidden $3\nu_4$ upper state by modeling the Octad and assigning $3\nu_4 - \nu_4$ transitions in the Pentad region. Now, it is clear that better modeling of Pentad intensity perturbations is essential for this tactic to succeed. Intensities for hundreds of transitions of each band are required, and there are currently too few measurements even for ν_1 and ν_3. Recovering ~1600 line intensities from Tarrago et al. would be helpful, but new measurements are still needed using path lengths that range through at least three orders of magnitude and at pressures high enough to maintain sample purity and stability. As highlighted in Table 5 of Butler et al. [7], the absolute accuracies of the measured intensities for the three polyads may be much worse (20 to 30%) than the experimental precisions (2 to 7%). This must be understood before a satisfactory global modeling of line intensities can be completed. The systematic differences between studies of the same bands may be caused by undetected impurities in the gas samples so that already-measured values could be normalized by a simple scaling. This point could be investigated at high resolution with a Bruker spectrometer configured with different detectors (MCT and InSb) to scan the different polyads in turn using an absorption cell holding the same sample throughout. Lower resolution cross sections of PH_3+N_2 mixtures recorded at PNNL [32] could provide some confirmation of relative intensities as well. In any case, the predictions produced by the present global analysis provide a good starting point for new intensity studies of PH_3 in the infrared.

5 Conclusion

The phosphine absorption spectrum in the 3 μm region has been modeled under high-resolution for the first time. This was achieved following a global approach in which the lower three polyads were fitted simultaneously using an effective hamiltonian in irreducible tensor form. A unique set of effective hamiltonian parameters has been determined. The precision obtained for the Pentad was significantly improved with respect to previous works. The precision for the Octad is not far from the experimental accuracy demonstrating that our model is well suited to account for the strong intra-polyad interactions encountered in the molecule. Except for the $3v_4$ band, the Octad vibrational sub-band origins are now well known. In particular, our fitted values remove any doubt about imprecise or erroneous values for the $v_1 + v_4$ and $v_3 + v_4$ sub-band origins that were reported by [5] and more recently by [16] and corrected in [19]. Our model open the way for a definitive analysis of the infrared spectrum of phosphine. Future progresses are expected from an exhaustive analysis of the intensities and the extension of the global fit to higher J values. Higher resolution experimental data would certainly be helpful to facilitate assignments and intensity measurements in the highly crowded high frequency edge of the Octad. An exhaustive line list of 55 223 calculated transitions at 296 K covering the region from 700 to 3500 cm^{-1}

has been calculated including all hot band lines arising from the Dyad upper states. It is available through the separate file `Line_List_296K.txt`. The newly calculated hot band transitions constitute already a substantial complement to the existing databases. In turn, the list will be submitted to complete or replace the previous empirical data in the HITRAN and GEISA databases.

From a more fundamental point of view, the comparison with the recent results of alternative *ab initio* studies indicates that the phosphine molecule is a good candidate to test the new theoretical approach presented by [20] and aimed at establishing a bridge between *ab initio* potential energy surfaces and effective hamiltonians on the basis of coherent tensorial formulations.

Acknowledgments

This work was supported by the Conseil Régional de Bourgogne. The research at Dijon and Tomsk was performed under the CNRS (France) and RFBR (Russia) PICS exchange program 05-05-22001a. Andrei Nikitin gratefully acknowledges support from the Russian program 2.10.1 *Optical Spectroscopy and Frequency Standards*. The research at the Jet Propulsion Laboratory (JPL), California Institute of Technology, was performed under contract with the National Aeronautics and Space Administration.

Appendix A. Supplementary material

Supplementary data associated with this article include a complete line list of 55 223 calculated transitions at 296 K, the list of the effective hamiltonian parameters, the list of the 38 effective dipole moment parameters for the Octad.

Appendix B. Sample line list

Table 10: Line list of the fitted positions in the region 3420 to 3430 cm^{-1}

The list below is extracted form the complete line list of 55 223 calculated transitions at 296 K from 700 to 3500 cm^{-1} available from the separate file `Line_List_296K.txt`. The 3420 to 3430 cm^{-1} window (plotted in Fig. 6) contains 340 calculated lines with intensities above 10^{-24} cm×molecule^{-1}. Only lines used for the present fit of positions are quoted in the Table.
(a) Calculated wavenumber in cm^{-1}.
(b) Obs-Calc residual for positions in $10^{-3}cm^{-1}$.
(c) Calculated intensity in cm×molecule^{-1} at 296 K.
(d) Relative residual for intensities in % .
(e) Vibrational assignment.
(f) Rotational assignment.
The rotational nomenclature quoted in the last column gives $^{\Delta K}\Delta J(J", K", C")$ where O, P, Q, R, S stand for ΔK (or ΔJ) $= -2, -1, 0, 1, 2$ respectively. $J", K", C"$ designate respectively the rotational quantum numbers and the ro-vibrational symmetry of the lower (initial) state of the transition.

Position (a)	(b)	Intensity (c)	(d)	(e)	(f)
3420.00757	4.1	0.12E-21	26.9	$\nu_1 + \nu_4(E)$	$^PQ(8,5,E)$
3420.03519	-2.9	0.24E-22	0.0	$\nu_3 + \nu_4(A_2)$	$^QQ(6,3,A1)$
3420.07010	2.0	0.19E-22	31.7	$\nu_3 + \nu_4(A_2)$	$^QQ(6,3,A2)$
3420.49575	-7.2	0.43E-22		$\nu_3 + \nu_4(A_2)$	$^QQ(7,3,A2)$
3420.57892	1.5	0.31E-22		$\nu_3 + \nu_4(A_2)$	$^QQ(7,3,A1)$
3420.60147	2.2	0.15E-21		$\nu_1 + \nu_4(E)$	$^PQ(4,4,E)$
3420.76789	-0.4	0.19E-21		$\nu_3 + \nu_4(E)$	$^RQ(10,1,E)$
3420.80677	-10.1	0.50E-22		$\nu_3 + \nu_4(A_2)$	$^QQ(8,3,A1)$
3420.93585	-2.2	0.25E-21	9.3	$\nu_3 + \nu_4(E)$	$^RQ(2,1,E)$
3420.95829	2.6	0.43E-22		$\nu_3 + \nu_4(A_2)$	$^QQ(9,3,A2)$
3420.97149	3.1	0.31E-22		$\nu_3 + \nu_4(A_2)$	$^QQ(8,3,A2)$
3421.13776	0.0	0.20E-21		$\nu_1 + \nu_4(E)$	$^PQ(5,4,E)$
3421.23628	-6.6	0.20E-22		$\nu_3 + \nu_4(A_2)$	$^QQ(9,3,A1)$
3421.24237	1.9	0.38E-21		$\nu_3 + \nu_4(E)$	$^RQ(3,1,E)$
3421.31808	-2.7	0.23E-22		$\nu_3 + \nu_4(A_2)$	$^QQ(2,2,E)$
3421.42108	-0.8	0.21E-21		$\nu_3 + \nu_4(A_2)$	$^RQ(6,1,E)$
3421.51181	1.6	0.28E-21		$\nu_3 + \nu_4(A_2)$	$^RQ(7,1,E)$
3421.56374	3.7	0.45E-21	-8.2	$\nu_3 + \nu_4(E)$	$^RQ(4,1,E)$
3421.67116	1.7	0.20E-21		$\nu_1 + \nu_4(E)$	$^PQ(6,4,E)$
3421.87870	-1.1	0.41E-21	2.2	$\nu_3 + \nu_4(E)$	$^RQ(5,1,E)$
3422.16428	-2.5	0.17E-21		$\nu_1 + \nu_4(E)$	$^PQ(7,4,E)$
3422.20766	-1.6	0.28E-21		$\nu_3 + \nu_4(E)$	$^RQ(6,1,E)$
3422.53376	2.0	0.16E-21		$\nu_3 + \nu_4(E)$	$^RQ(7,1,E)$
3422.56973	0.3	0.12E-21	16.4	$\nu_3 + \nu_4(A_1)$	$^QP(2,0,A1)$

Position (a)	(b)	Intensity (c)	(d)	(e)	(f)
3422.59464	-6.8	0.12E-21		$\nu_1 + \nu_4(E)$	$^PQ(8, 4, E)$
3422.70400	-1.2	0.40E-22		$\nu_3 + \nu_4(A_2)$	$^QQ(5, 2, E)$
3422.81516	2.2	0.18E-21		$\nu_1 + \nu_4(E)$	$^PQ(3, 3, A2)$
3422.83786	0.7	0.18E-21	15.7	$\nu_1 + \nu_4(E)$	$^PQ(3, 3, A1)$
3422.86311	-4.4	0.57E-22		$\nu_3 + \nu_4(A_2)$	$^RQ(9, 1, E)$
3422.97173	0.5	0.71E-22		$\nu_1 + \nu_4(E)$	$^PQ(9, 4, E)$
3423.00186	-1.7	0.58E-22		$\nu_3 + \nu_4(A_2)$	$^QQ(6, 2, E)$
3423.08553	2.0	0.55E-22		$\nu_3 + \nu_4(A_2)$	$^QQ(7, 2, E)$
3423.22134	5.4	0.25E-21	-0.3	$\nu_1 + \nu_4(E)$	$^PQ(4, 3, A1)$
3423.29151	-2.6	0.26E-21	2.0	$\nu_1 + \nu_4(E)$	$^PQ(4, 3, A2)$
3423.36253	2.8	0.24E-21	14.0	$\nu_1 + \nu_4(E)$	$^RQ(9, 0, A2)$
3423.39201	1.5	0.87E-22	17.6	$\nu_3 + \nu_4(A_1)$	$^QP(2, 1, E)$
3423.53185	-6.4	0.14E-22		$\nu_1 + \nu_4(E)$	$^QQ(4, 1, E)$
3423.59480	-9.4	0.39E-21		$\nu_1 + \nu_4(E)$	$^RQ(8, 0, A1)$
3423.62301	3.5	0.25E-21		$\nu_1 + \nu_4(E)$	$^PQ(5, 3, A2)$
3423.78738	-1.7	0.54E-21		$\nu_1 + \nu_4(E)$	$^RQ(7, 0, A2)$
3423.81508	2.4	0.36E-22		$\nu_1 + \nu_4(E)$	$^QQ(5, 1, E)$
3423.91007	5.6	0.66E-21		$\nu_3 + \nu_4(E)$	$^RQ(6, 0, A1)$
3423.93950	3.4	0.74E-21		$\nu_3 + \nu_4(E)$	$^RQ(3, 0, A2)$
3423.97549	1.4	0.21E-21		$\nu_1 + \nu_4(E)$	$^PQ(6, 3, A1)$
3424.05335	12.8	0.55E-22		$\nu_1 + \nu_4(E)$	$^QQ(6, 1, E)$
3424.10747	2.6	0.24E-22		$\nu_3 + \nu_4(E)$	$^QQ(7, 2, E)$
3424.21984	12.3	0.58E-22		$\nu_1 + \nu_4(E)$	$^QQ(7, 1, E)$
3424.24813	-2.8	0.14E-21	23.1	$\nu_1 + \nu_4(E)$	$^PQ(7, 3, A2)$
3424.29358	-3.7	0.24E-21	20.8	$\nu_1 + \nu_4(E)$	$^PQ(6, 3, A2)$
3424.31162	-0.9	0.43E-22		$\nu_1 + \nu_4(E)$	$^QQ(8, 1, E)$
3424.33843	6.3	0.30E-22		$\nu_3 + \nu_4(A_2)$	$^QQ(8, 2, E)$
3424.40499	0.2	0.12E-22		$\nu_1 + \nu_4(E)$	$^PQ(10, 3, A1)$
3424.42092	-3.6	0.83E-22		$\nu_1 + \nu_4(E)$	$^PQ(8, 3, A1)$
3424.47524	0.3	0.38E-22		$\nu_1 + \nu_4(E)$	$^PQ(9, 3, A2)$
3424.55615	-4.8	0.21E-21		$\nu_1 + \nu_4(E)$	$^PQ(2, 2, E)$
3424.63120	-4.0	0.47E-22	12.3	$\nu_3 + \nu_4(A_2)$	$^QQ(1, 0, A2)$
3424.77816	1.8	0.19E-21	16.4	$\nu_1 + \nu_4(E)$	$^PQ(7, 3, A1)$
3424.83193	-7.3	0.29E-21	4.1	$\nu_1 + \nu_4(E)$	$^PQ(3, 2, E)$
3424.96469	-1.2	0.11E-21	13.5	$\nu_3 + \nu_4(A_2)$	$^QQ(2, 0, A1)$
3425.05424	5.3	0.50E-22		$\nu_3 + \nu_4(A_2)$	$^QQ(4, 1, E)$
3425.12384	-6.5	0.28E-21	4.9	$\nu_1 + \nu_4(E)$	$^PQ(4, 2, E)$
3425.20859	5.3	0.13E-21		$\nu_1 + \nu_4(E)$	$^PQ(8, 3, A2)$

Position (a)	(b)	Intensity (c)	(d)	(e)	(f)
3425.28669	-4.4	0.24E-21	1.1	$\nu_1+\nu_4(E)$	${}^PQ(1,1,E)$
3425.38839	0.2	0.16E-21	15.9	$\nu_3+\nu_4(A_2)$	${}^QQ(3,0,A2)$
3425.40196	1.3	0.23E-21	7.6	$\nu_1+\nu_4(E)$	${}^PQ(5,2,E)$
3425.54318	1.6	0.35E-21	-4.7	$\nu_1+\nu_4(E)$	${}^PQ(2,1,E)$
3425.55844	-1.8	0.82E-22		$\nu_1+\nu_4(E)$	${}^PQ(9,3,A1)$
3425.63413	13.1	0.17E-21	5.2	$\nu_1+\nu_4(E)$	${}^PQ(6,2,E)$
3425.71314	2.1	0.78E-22		$\nu_3+\nu_4(A_2)$	${}^QQ(5,1,E)$
3425.79355	12.9	0.10E-21	-10.4	$\nu_1+\nu_4(E)$	${}^PQ(7,2,E)$
3425.91545	6.6	0.37E-21	-25.0	$\nu_1+\nu_4(E)$	${}^PQ(3,1,E)$
3426.03327	2.6	0.27E-22		$\nu_3+\nu_4(A_2)$	${}^PQ(3,2,E)$
3426.34599	-1.9	0.85E-22		$\nu_3+\nu_4(A_2)$	${}^QQ(6,1,E)$
3426.34970	-7.7	0.16E-21		$\nu_3+\nu_4(A_2)$	${}^QQ(5,0,A2)$
3426.39126	9.0	0.32E-21	3.9	$\nu_1+\nu_4(E)$	${}^PQ(4,1,E)$
3426.64622	4.6	0.49E-22		$\nu_3+\nu_4(A_2)$	${}^PQ(4,2,E)$
3426.80220	-9.1	0.13E-21	6.9	$\nu_3+\nu_4(A_2)$	${}^QQ(6,0,A1)$
3426.89896	2.5	0.68E-22	-2.2	$\nu_3+\nu_4(A_2)$	${}^QQ(7,1,E)$
3426.94821	5.6	0.23E-21	-2.0	$\nu_1+\nu_4(E)$	${}^PQ(5,1,E)$
3427.01836	1.6	0.22E-23		$\nu_3+\nu_4(E)$	${}^OQ(7,7,E)$
3427.18124	-11.5	0.92E-22	11.4	$\nu_3+\nu_4(A_2)$	${}^QQ(7,0,A2)$
3427.30001	2.7	0.59E-22		$\nu_3+\nu_4(A_2)$	${}^PQ(5,2,E)$
3427.33000	5.7	0.42E-22		$\nu_3+\nu_4(A_2)$	${}^QQ(8,1,E)$
3427.48521	10.5	0.49E-22		$\nu_3+\nu_4(A_2)$	${}^QQ(8,0,A1)$
3427.54081	-2.9	0.13E-21		$\nu_1+\nu_4(E)$	${}^PQ(6,1,E)$
3427.64909	-4.7	0.26E-23		$\nu_3+\nu_4(E)$	${}^OQ(8,7,E)$
3427.92677	0.0	0.54E-22		$\nu_3+\nu_4(A_2)$	${}^PQ(6,2,E)$
3428.10076	-9.6	0.67E-22		$\nu_1+\nu_4(E)$	${}^PQ(7,1,E)$
3428.47267	2.0	0.39E-22		$\nu_3+\nu_4(A_2)$	${}^PQ(7,2,E)$
3428.51372	-1.9	0.39E-23		$\nu_1+\nu_4(E)$	${}^OQ(7,3,A2)$
3428.54605	-5.5	0.56E-23		$\nu_3+\nu_4(E)$	${}^OQ(7,6,A1)$
3428.56092	-9.0	0.28E-22		$\nu_1+\nu_4(E)$	${}^PQ(8,1,E)$
3428.65750	6.4	0.73E-23	84.6	$\nu_3+\nu_4(E)$	${}^OQ(6,3,A1)$
3428.88159	3.1	0.90E-23		$\nu_1+\nu_4(E)$	${}^PQ(9,1,E)$
3428.93079	15.3	0.50E-23		$\nu_3+\nu_4(E)$	${}^OQ(8,6,A2)$
3429.00603	-0.5	0.42E-23		$\nu_3+\nu_4(E)$	${}^OQ(5,5,E)$
3429.36290	-7.6	0.84E-23		$\nu_3+\nu_4(E)$	${}^OQ(6,5,E)$
3429.64004	-5.3	0.94E-23		$\nu_3+\nu_4(E)$	${}^OQ(7,5,E)$
3429.67447	-9.4	0.96E-23		$\nu_1+\nu_4(E)$	${}^OQ(7,2,E)$
3429.81323	0.9	0.26E-23		$\nu_3+\nu_4(E)$	${}^OQ(9,5,E)$

Position (a)	(b)	Intensity (c)	(d)	(e)	(f)
3429.83826	-1.3	0.86E-23		$\nu_3 + \nu_4(E)$	${}^{O}Q(5, 4, E)$
3429.99636	-1.4	0.28E-23		$\nu_3 + \nu_4(E)$	${}^{O}Q(3, 3, A1)$

List of Tables

List of Figures

References

[1] G. Tarrago, N. Lacome, A. Levy, G. Guelachvili, B. Bezard, P. Drossart, J. Mol. Spectrosc. 154 (1992) 30–42. 1, 2, 3, 6, 11, 12, 14

[2] L. Fusina, M. Carlotti, J. Mol. Spectrosc. 130(2) (1988) 371–381. 1, 2, 3, 12

[3] L. Fusina, G. Di Lonardo, J. Mol. Structure 517 (2000) 67–78. 1, 2, 11, 12, 14

[4] L.R. Brown, R.L. Sams, I. Kleiner, C. Cottaz, L. Sagui, J. Mol. Spectrosc. 215 (2002) 178–203. 1, 2, 3

[5] O.N. Ulenikov, E.S. Bekhtereva, V.A. Kozinskaia, J.J. Zheng, S.G. He, S.M. Hu, Q.S. Zhu, C. Leroy, L. Pluchart, L. J. Quant. Spectrosc. Radiat. Transfer 83 (2004) 599–618. 1, 19

[6] O.N. Ulenikov, Y.B. Yuhnik, E.S. Bekhtereva, N.E. Tyabaeva, H. Burger, W. Jerzembeck, L. Fusina, J. Mol. Spectrosc. 224 (2004) 194–195. 1

[7] R.A.H. Butler, L. Sagui, I. Kleiner, L.R. Brown, J. Mol. Spectrosc. 238 (2006) 178–192. 1, 2, 3, 11, 12, 14, 16, 18, 19

[8] L.S. Rothman, D. Jacquemart, A. Barbe, D.C. Benner, M. Birk, L.R. Brown, M.R. Carleer, C. Chackerian, K. Chance, L. Coudert, V. Dana, V.M. Devi, J.M. Flaud, R.R. Gamache, A. Goldman, J.-M. Hartmann, K.W. Jucks, A.G. Maki, J.-Y. Mandin, S.T. Massie, J. Orphal, A. Perrin, C.P. Rinsland, M.A.H. Smith, J. Tennyson, R.N. Tolchenov, R.A. Toth, J. Van der Auwera, P. Varanasi, G. Wagner, G., J. Quant. Spectrosc. Radiat. Transfer 96 (2005) 139–204. 2, 3, 18

[9] N. Jacquinet-Husson, N.A. Scott, A. Chedina, L. Crepeau, R. Armante, V. Capelle, J. Orphal, A. Coustenis, C. Boonne, N. Poulet-Crovisier, A. Barbe, M. Birk, L.R. Brown, C. Camy-Peyret, C. Claveau, K. Chance, N. Christidis, C. Clerbaux, P.F. Coheur, V. Dana, L. Daumont, M.-R. De Backer-Barilly, G. Di Lonardo, J.M. Flaud, A. Goldman, A. Hamdouni, M. Hess, M.D. Hurley, D. Jacquemart, I. Kleiner, P. Kopke, J.-Y. Mandin, S. Massie, S. Mikhailenko, S. Nemtchinov, A. Nikitin, D. Newnham, A. Perrin, V.I. Perevalov, S. Pinnock, L. Regalia-Jarlot, C.P. Rinsland, A. Rublev, F. Schreier, L. Schult, K.M. Smith, S.A. Tashkun, J.-L. Teffo, R.A. Toth, Vl.G. Tyuterev, J. Van der Auwera, P. Varanasi, G. Wagner, J. Quant. Spectrosc. Radiat. Transfer 109 (2008) 1043–1059. 2

[10] J.-P. Champion. Can. J. Phys. 55 (1977) 1802–1028. 2, 4

[11] C. Wenger, J.-P. Champion, J. Quant. Spectrosc. Radiat. Transfer 59 (1998) 471–480. 2

[12] A. Nikitin, J.-P. Champion, Vl.G. Tyuterev, J. Mol. Spectrosc. 182 (1997) 72-84. 2, 8

[13] A. Nikitin, J.-P. Champion, Vl.G. Tyuterev, J. Quant. Spectrosc. Radiat. Transfer 82 (2003) 239–249. 2, 8

[14] V. Boudon, J.-P. Champion, T. Gabard, M. Loete, F. Michelot, G. Pierre, M. Rotger, C. Wenger, M. Rey, J. Mol. Spectrosc. 228 (2004) 620–634. 2, 4

[15] D. Wang, Q. Shi, Q.S. Zhu, J. Chem. Phys. 112 (2000) 9624–9631. 2

[16] S.N. Yurchenko, M. Carvajal, W. Thiel, P. Jensen, J. Mol. Spectrosc. 239 (2006) 71–87. 2, 19

[17] S.N. Yurchenko, W. Thiel, P. Jensen, J. Mol. Spectrosc. 245 (2007) 126–140. 2

[18] S.N. Yurchenko, W. Thiel, M. Carvajal, P. Jensen, Chem. Phys. (2008) 346 (2008) 146–159. 2

[19] R.I. Ovsyannikov, W. Thiel, S.N. Yurchenko, M. Carvajal, P. Jensen, J. Chem. Phys. 129 (2008) 044309. 2, 4, 7, 19

[20] M. Rey, A. Nikitin, Vl.G. Tyuterev, F. Holka, 20th international conference on High Resolution Molecular Spectroscopy Prague september 2-6, Poster D51, 2008. 2, 4, 7, 20

[21] R.I. Ovsyannikov, W. Thiel, S.N. Yurchenko, M. Carvajal, P. Jensen, J. Mol. Spectrosc. 252 (2008) 121–128. 2, 12, 13, 15

[22] A.G. Maki, L.S. Wells, Wavenumber Calibration Tables from Heterodyne Frequency Measurements, NIST Special Publication 821. U.S. Government Printing Office, Washington, DC, 1991. 2, 3

[23] C.R. Pollock, F.R Petersen, D.A. Jennings, J.S. Wells, A.G. Maki, J. Mol. Spectrosc. 99 (1983) 357–368. 2, 3

[24] S. Albert, S. Bauerecker, V. Boudon, L.R. Brown, J.-P. Champion, M. Loete, A. Nikitin, M. Quack, Chem. Phys. xxx (2008) xxx-xxx : doi:10.1016/J.chemphys.2008.10.019. 4, 8

[25] J.-P. Champion, M. Loete, G. Pierre, Spherical Top Spectra, in: K.N. Rao & A. Weber (Eds.), Spectroscopy of the Earth's atmosphere and interstellar medium, Academic Press, Columbus, 1992, pp. 339-422. 4, 8

[26] A. Nikitin, J.-P. Champion, Vl.G. Tyuterev, L.R. Brown, G. Mellau, M. Lock, J. Mol. Structure 517 (2000) 1–24. 4

[27] A. Nikitin, L.R. Brown, L. Fejard, J.-P. Champion, Vl.G. Tyuterev, J. Mol. Spectrosc. 216 (2002) 225-251. 4

[28] A. Nikitin, J.-P. Champion, L.R. Brown, J. Mol. Spectrosc. 240 (2006) 14-25. 4

[29] A. Nikitin, J.-P. Champion, J. Mol. Spectrosc. 230 (2005) 168–173. 4

[30] A. Nikitin, J.-P. Champion, H. Burger, J. Mol. Spectrosc. 230 (2005) 174–184. 4

[31] E. Lobodenko, O. Sulakshina, V. Perevalov, Vl.G. Tyuterev, J. Mol. Spectrosc. 126 (1987) 159–170. 9

[32] S.W. Sharpe, T.J. Johnson, R.L. Sams, P.M. Chu, G.C. Rhoderick, P.A. Johnson, Applied Spectroscopy 58 (2004) 1452–1461.

2, 19